Fabrication of integrated diffractive micro-optics for MEMS applications

L. R. Senesac[a], R. H. Farahi[b], J. L. Corbeil[b], D. D. Earl[b], S. Rajic[b], and P. G. Datskos[b]

[a] University of Tennessee, 401 Nielsen Physics Bldg., Knoxville, TN 37996-1200
[b] Oak Ridge National Laboratory, P.O. Box 2008, Oak Ridge, TN 37831-8039

ABSTRACT

We investigated the fabrication of integrated diffractive micro-optical features on MEMS structures for the purpose of motion detection. The process of producing the diffractive features and the MEMS structures by focused ion beam milling is described in detail, as is the ion beam sputtering process used to produce coatings on these structures. The diffractive features of the circular Fresnel zone plate (FZP) and spiral FZP were fabricated on MEMS structures and the relevant diffraction theory is discussed. The spiral FZP diffractive features produced well defined foci whose intensity varies with distance from the FZP. Observation of these intensity variations enabled us to detect the motion of the MEMS structure, and the resulting device was used to scan an IR image of a hot object.

Keywords: optical readout, MEMS, diffraction, Fresnel zone plate, IR imaging

1. INTRODUCTION

For a wide range of micro-electro-mechanical-systems (MEMS) it is desirable to accurately measure the position or motion of a small structure. Although there are ways to obtain an electrical output signal corresponding to micro-mechanical deflection of such devices (capacitive, resistive, etc.), it would be preferable to eliminate the complex two dimensional array of contacts and cross connects involved in typical multiplexed readout schemes. For this reason, the simplicity of a non-contact optical readout approach will prove more useful for many applications. The particular optical approach we employ is based on diffraction effects of Fresnel zone micro-optical features located within the MEMS structure.

Positional changes of less than 0.1 nm are routinely measured in atomic force microscopy (AFM) technology. There are a number of possible readout schemes that can be adopted for this scale of position determination: electron tunneling, capacitive, resistive, piezoresistive, piezoelectric, and optical [1]. Optical methods such as direct ray reflection, interferometry, and diffraction are extremely sensitive and can have low power consumption. In a diffractive readout the motion of the diffractive structure produces intensity changes from an incoming beam of collimated laser light and these changes can be mapped with a simple CCD device to form a completely non-contact optical readout scheme. Direct ray reflection methods require that both the incident beam to the device and the reflected light to the detector be on the same side of the device. The diffractive features, however, can be read from either reflection or transmission of the incident light.

In the present work we discuss the relevant Fresnel optics behind the diffractive elements used, the fabrication processes utilized in their construction, and some preliminary testing of the finished devices with a CCD based diffractive optical readout.

2. FRESNEL ZONE THEORY

The diffractive elements discussed herein are of two basic structure types. The first is the circular Fresnel zone plate (FZP), and the second type is the spiral FZP. Both structures utilize Fresnel near-field diffraction to produce interference maxima at specific points or foci along or near to the optical axis of the device.

Correspondence: E-mail: lrs@ornl.gov; Telephone: (865) 241-3118; Fax: (865) 574-9407

2.1 Circular Fresnel zone plate

A circular FZP is shown in Figure 1. The radius of each successive circular boundary between the light and dark regions is given by $R_m = m^{1/2} R_1$, where R_1 is the radius of the central circle [2]. For transmission of collimated laser light through the FZP, the dark areas block the light while the light rings allow its transmission and interfere constructively on the axis of the FZP at the primary focus. This focus distance is given by $f = R_1^2 / \lambda$, where λ is the wavelength of the incident light [2]. Each transmission region is called a ring and therefore the FZP in Figure 1 has 12 rings. Two different FZPs, with equal R_1 but one having 8 rings and the other having 12 rings, were analyzed for the arbitrary parameters λ = 632.8 nm, and R_1 = .001 m. The focusing characteristics of each FZP were calculated [3] and the results for the 8 and 12 ring cases are compared in Figure 2. From Figure 2 it can be seen that as the number of concentric rings in an FZP is increased, the intensity of the FZP's focus is increased and the width of the focus decreased.

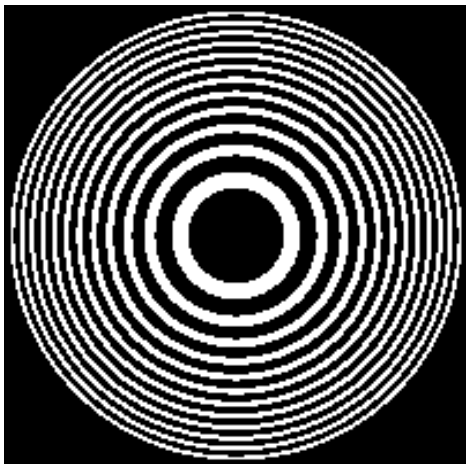

Figure 1. Milling template for a 12-ring circular FZP.

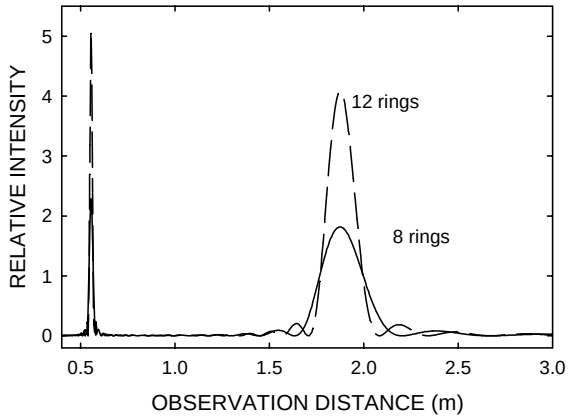

Figure 2. Intensity profile along the optical axis from an 8 and 12-ring circular FZP.

2.2 Spiral Fresnel zone plates

The spiral FZP shown in Figure 3 has the advantage of not requiring any additional support structure. The spiral FZP has a transmission profile similar to that of the circular FZP [3]. Two different spiral FZPs with equal R_1 ,one with 8 rings and one with 12 rings, were analyzed for the arbitrary parameters λ = 632.8 nm, and R_1 = .001 m. The focusing characteristics of each FZP were calculated [3] and the results for the 8 and 12 ring cases are compared in Figure 4. A comparison with Figure 2 shows that the foci of the spiral FZP occur at nearly the same distance as for the circular FZP.

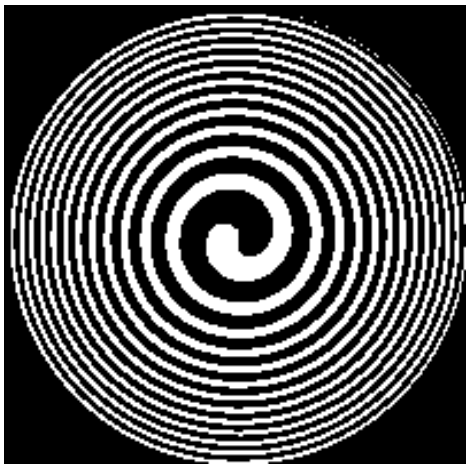

Figure 3. Milling template for a 12-ring spiral FZP

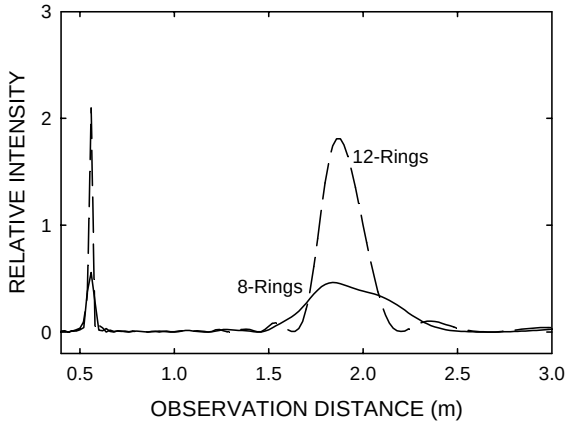

Figure 4. Intensity profile along the optical axis from an 8 and 12-ring spiral FZP.

2.3 Spatial resolution characteristics of micro-FZP

To examine the characteristics of a micro-FZP we chose to model a circular FZP with eight concentric rings, and R_1 = 6.25 μm (total diameter = 50 μm). The intensity profile along the optical axis was calculated for the typical experimental conditions; λ = 632.8 nm, and R_1 = 6.25 μm, and is shown in Figure 5. The primary focus is located at 61.0 μm. The full-width-at-half-maximum for the peak in Figure 5 is approximately 9 μm. The focused spot diameter was calculated to be roughly 4 μm. With a microscope attached to a CCD this spot size can easily be expanded to illuminate a 3x3 or 4x4 pixel area on the CCD. Since the distance between the brightest point at the peak and the darkest point at the base is about 8 μm, the corresponding change in spot intensity represents an 8 μm motion of the device. For a single 8-bit CCD pixel the difference between bright and dark can have as many as 256 levels, for a 12-bit CCD, 4096 levels. If the spot covers a 3x3 pixel area, a difference of over 36,000 levels is possible provided a sufficiently high signal to noise ratio can be obtained. For an intensity range of 8 μm and 10,000 levels of sensitivity, motions of less than 1 nm may be measured.

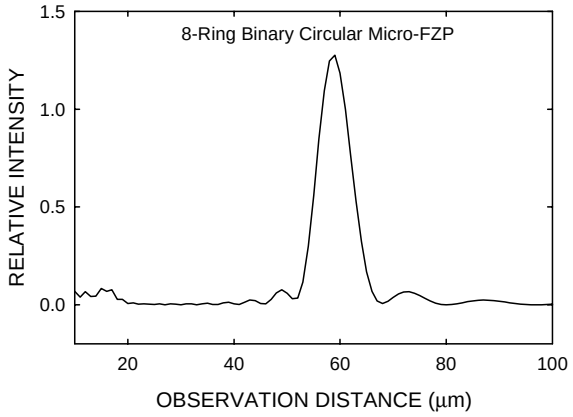

Figure 5. Intensity profile along the optical axis for a 50-μm diameter micro-FZP.

3. FABRICATION OF DIFFRACTIVE STRUCTURES

Our current projects require a MEMS device which is sensitive to visible and thermal photons. For this sensitivity we rely on the thermal induced stress due to the bi-material effect. If a microstructure is composed of two layers of material which have different rates of thermal expansion, the device will change shape as its temperature changes [4]. As the microstructure is exposed to and absorbs thermal photons, the temperature increase produces a bending motion of the structure which we detect optically with the aid of the integrated diffractive micro-optics. For this reason, the first step in the fabrication process is to apply a coating of a suitable material to the raw material substrate and thereby create a stable bi-material stock from which to pattern the device.

3.1 Bi-material coating process

The devices discussed here are of two main shapes: planar square pixel, and planar triangular cantilever. The process typically starts with a 500 nm thick substrate of Si or SiNx. For the bi-material coating we have had good success with Al, Au, and Zn with coating thicknesses from 50 nm to about 200 nm. The coatings were applied by physical sputtering using a Commonwealth Scientific Corporation Model II 3 cm broad-beam ion source and ID-2500 power supply. The source produces a steady 3 cm beam of argon ions which strike the target made of the required coating material. This target material is then sputtered onto the object to be coated.

We found that if a thick coating is rapidly applied to one side of the substrate, the result is often a badly deformed sheet. If the coating is applied in thin layers with time for the sheet to cool between coatings, a flat sheet of bi-material can be produced. The exact thickness per coating varies from 10 nm to 20 nm depending on the materials used and on the thickness of the initial substrate. The cooling time also varies, but 5 to 10 minutes is usually sufficient. For coating thicknesses which are a significant fraction of the substrate thickness, some deformation of the substrate is difficult to avoid with the layering method.

Another method that works well for producing a flat substrate is rotational coating. If the substrate is mounted so that it can be rotated at a slow rate during the sputtering process, an even coating is applied to all sides. For the bi-material effect to still work, the coating must then be removed from one side of the substrate. For thick coatings applied in one layer, the substrate sometimes bends after the coating is removed from one side due to thermal stresses created during the rapid sputtering process. This problem can usually be avoided by rotationally coating in layers of 30 nm to 40 nm with brief 5 to 10 minute pauses between layers to allow cooling. For thick coatings the rotational method almost always produced a flatter substrate.

3.2 Focused ion beam (FIB) milling

To pattern the microstructures with integrated micro-optics from the coated substrate we employ the FEI focused ion beam (FIB) Model 200 Series Workstation. The object to be milled is placed on a multi-axis stage inside a vacuum chamber. On top of the chamber is the FIB column which produces, focuses, and scans the beam of ions. A strong electric field (~10^8 V/cm) is applied to a gallium liquid metal ion source to extract positively charged gallium ions downward through the FIB column. The stream of ions passes through two electrostatic lenses, a steering quadrupole and an octupole deflector, which focus the ions into a beam and scan the beam over the target. As the ion beam strikes the target, material is removed through the physical sputtering process. The ions striking the target surface also generate secondary electrons and ions which may then be detected and processed to form an image of the target area scanned by the focused ion beam.

A variable aperture allows ion beam widths from 18 nm to 600 nm with beam currents from 1 pA to 11,500 pA respectively. The material removal rate varies with the hardness of the target material, but typical removal for silicon is from 0.0006 to 1.7 cubic microns per second for the 18 nm and 600 nm beams respectively. For a softer material such as gold the removal rate is about five times faster.

The FIB 200 video monitor displays a 1024 x 1024 image of the stage and target and the image magnification is variable from 63X to 100kX. The ion beam scanning system divides the current viewing area into a 4096 x 4096 grid. The beam can be moved to any point on this grid and stay there for a programmable dwell time. A bitmap image of the feature to be milled is created and the FIB 200 software uses this bitmap to make an array of milling points on the 4096 x 4096 grid. The number and position of these milling points depends on the chosen beam size and magnification. Simple shapes (straight lines, boxes, etc.) are also available from a drawing menu for quick milling.

3.3 Fabrication of a pixel with integrated 4-ring spiral FZP

The fabrication of the device in Figure 6 began with a SiNx substrate approximately 150 μm wide, 70 μm high, and 500 nm thick. The substrate was then rotationally coated (as outlined above) with 100 nm of Zn. The coating was applied in three layers with five minutes of sputtering per layer and a five minute pause between layers. The result was a very flat sheet with no noticeable bending.

The first feature to be milled is the 4-ring spiral FZP. The primary radius R_1 = 5 μm and the diameter is about 30 μm. The spiral is a very delicate structure. At the thinnest point it is less than 2 μm wide, and this point must carry the entire weight of the spiral. This is not a problem of strength however because at this scale structures are many times stronger than an object of similar proportion would be on the macro scale. The problem is that it makes the spiral very prone to vibrational motion. Once the spiral shape starts to mill all the way through, if the free parts of the spiral start to move while the pattern is still milling, these free parts will move into the beam and be milled away. Experience has shown that delicate structures like the spiral should be milled first while the substrate is as rigid as possible so that the spiral will remain still until the milling process is completed. A beam diameter of 120 nm was used at a magnification of 3500X. The center area of the spiral started milling through at about 12 minutes, but it took 26 minutes total for the entire shape to finish and look clean.

The leg structure was milled next with the same beam size and the total milling time for this step was 23 minutes. Since the pixel is still surrounded by material, it remains fairly still during this milling process. Finally the top and side waste are cut away from the pixel leaving behind a very sensitive microstructure. The Zn is next removed from one side of the entire pixel by drawing a solid milling box shape over the area and milling uniformly until the Zn is removed.

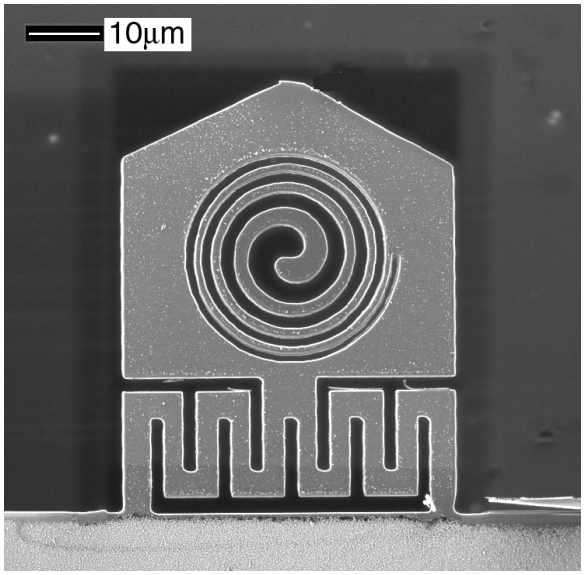

Figure 6. FIB image of pixel with 4-ring spiral FZP

3.4 Fabrication of a pixel with integrated 8-ring circular FZP

The device shown in Figure 7 began as a SiNx substrate blank similar to the pixel above, but was rotationally coated with 200 nm of Zn. The coating was applied in six layers with five minutes of sputtering per layer and a five minute pause between layers. For the circular FZP, the structure is not milled all the way through since the circular FZP can not support itself. With this device we use the SiNx substrate because the visible laser light will pass through it with little reflection. The zinc coating however reflects this light very well. Therefore if the circular FZP pattern is milled through the zinc coating but not through the substrate, the device will still focus the laser light either in transmission through the SiNx or in reflection from the zinc.

When the FIB system is used to image a device some of the entire surface of the device is milled away as the secondary electrons are produced for the imaging. For most viewing with low beam currents this effect is of little consequence, however, if the surface is a thin coating of a soft material, the surface coating may be removed by prolonged imaging. For this device the leg structure chosen is more complex and time consuming to mill than in the previous example. Also, the time needed to mill the FZP into the soft zinc is quite short. If the FZP is milled first, there is a chance that it will be degraded by the imaging process needed to mill the leg section. Therefore the leg structures were milled first

We started milling on the back side first to minimize the inadvertent sputtering of the front side zinc coating. The vertical lines of the legs were milled with a beam width of 100 nm and took about 25 minutes. Next, alternate legs were milled through the zinc coating and half way through the SiNx (about 250 nm) to thin the legs (note the dark rectangles on the alternate legs in Figure 7). Each leg was milled for 2.5 minutes with the same 100 nm beam width. The horizontal line at the top of the legs was then milled through, and all the zinc was removed from the back of the head area so that light will transmit through. This large area only required about 8 minutes to remove the 200 nm of zinc. The device was then turned over to the front side (shown in Figure 7) and the alternating legs were thinned by the same method as before, but to the opposite legs from those thinned on the back side. After several trial runs, the 8-ring FZP was then milled through the zinc with the 100 nm beam in 90 seconds. Finally the pixel was turned again to the back side, the bottoms of the legs were released, and the pixel was released from the top and side waste.

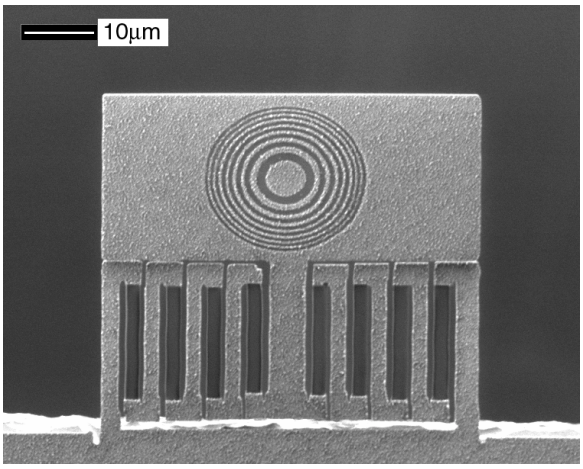

Figure 7. FIB image of pixel with 8-ring circular FZP. The head of the pixel is rotated forward giving the FZP a slightly elliptical appearance.

3.5 Fabrication of triangular cantilevers with FZP

The square pixels above are well suited for use in arrays such as those used in imaging, however a simple triangular cantilever serves well when only a single device is required. A bi-material triangular cantilever can in general be made more responsive to temperature changes simply by increasing the length of the legs.

Figure 8 is an example of a SiNx triangular cantilever with legs of 250 µm length. The legs are not shown so that the FZP can be better imaged. The SiNx is 500 nm thick and is coated on one side with a 40 nm layer of gold. In the head of the triangle is milled a 4-ring spiral FZP with a diameter of 36 µm. The milling process for this device is essentially identical to the 4-ring spiral FZP in the pixel discussed above. Figure 9 shows a similar cantilever with a 9-ring circular FZP milled only through the gold layer.

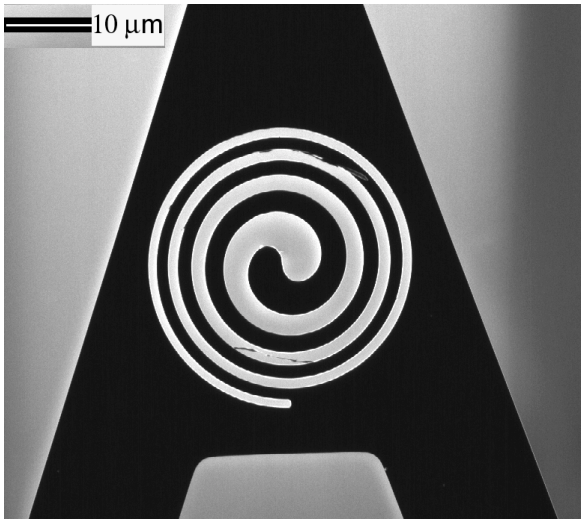

Figure 8. FIB image of triangular cantilever with 4-ring spiral FZP.

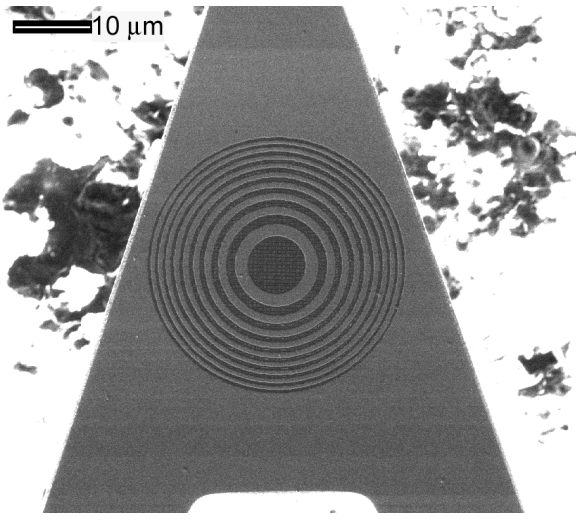

Figure 9. FIB image of triangular cantilever with 9-ring circular FZP.

4. DEVICE TESTING

4.1 Experimental set-up

Several types of tests were performed with the finished FZP devices ranging from simply imaging the device focusing characteristics, to using them as active IR pixels to produce an image of a hot object. In the experimental set-up (Figure 10) it was necessary to irradiate the device with an IR source and at the same time illuminate it with a readout diode laser while observing the FZP with a CCD. The IR source is sometimes an IR black-body source with temperature settings from room temperature to over 1000 degrees C, but for many of the tests a simple variable temperature soldering iron was used. In either case the heat source was placed such that its radiation was imaged onto the FZP device by a diamond turned aluminum mirror. A rotating aperture was placed near the source to allow chopping of the signal when desired. A germanium beamsplitter was positioned as shown in Figure 10 so that the IR radiation could pass through it to the FZP device, but it also serves as an excellent mirror for the collimated beam from the diode laser. The laser beam illuminated the device and the diffraction pattern from the FZP micro-optic was then imaged onto a CCD by a microscope. The microscope images the device through a 2 μm pinhole placed near to but outside the primary focus of the FZP diffractive structure. The pinhole restricts the field of view to the area immediately around the focus of the FZP structure and also prevents the collimated laser light from saturating the CCD. A 671 nm narrow pass filter was installed between the microscope and the CCD to greatly reduce the CCD exposure to light from any source other than the laser. The CCD used was a 12-bit 1000x1000 pixel CCD and was connected to a digital image acquisition board and computer.

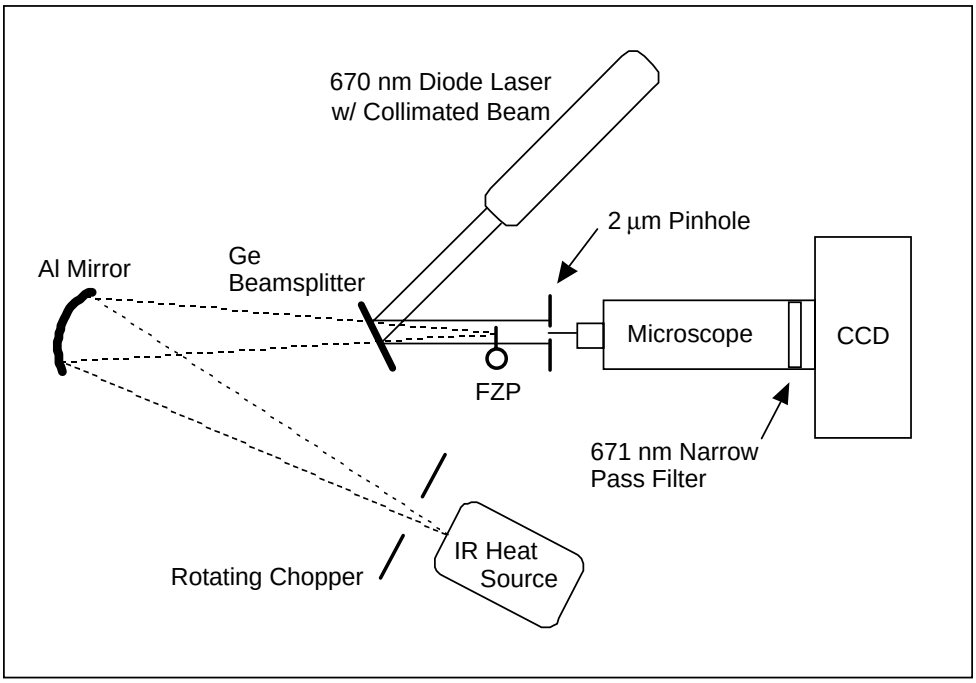

Figure 10. Diagram of the experimental set-up.

4.2 Observation of FZP device focus

The 4-ring spiral FZP described in Section 3.3 above was mounted into the experimental set-up as shown in Figure 10. Collimated light from the diode laser illuminated the FZP and the diffraction pattern was viewed with the microscope/CCD camera. No IR source or chopper was used for this test. For an ideal FZP with a primary radius of 5 μm illuminated with a 670 nm laser, the primary focus was predicted to be found at a distance of 37.3 μm from the device plane. The camera was first focused on the spiral plane and then moved out until the diffraction focus was sharpest. The focus for this device was found to be at a distance of about 40 μm and an image of the focus spot can be seen in the right image in Figure 11. The left image in Figure 11shows the device while still in the FIB at the same magnification for comparison.

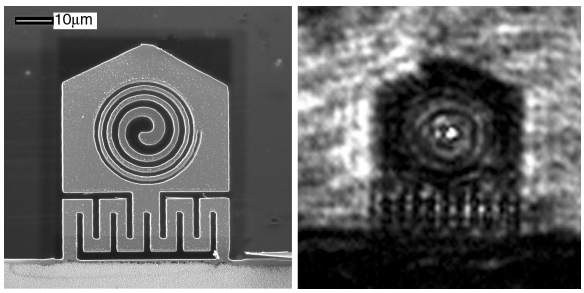

Figure 11. Left image: FIB image of the 4-ring spiral FZP. Right image: Laser light diffraction image of device focus.

Similarly, the 4-ring spiral FZP described in Section 3.5 was tested and was also found to exhibit a satisfactory focus spot. In Figure 12 are: the FIB image shown for comparison (left), the laser back illuminated image of the spiral FZP focused at the spiral plane (center), and the laser back illuminated image of the device at the plane of focus (right). For this device the primary radius R_1 = 6 μm and therefore the theoretical primary focus is at about 54 μm. The primary focus for this device however, was found at 100 μm.

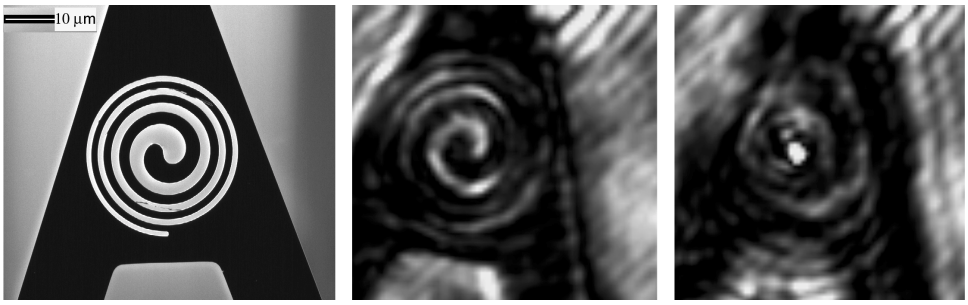

Figure 12. Left image: FIB image of the 4-ring spiral FZP on a triangular cantilever. Center image: Laser light image of spiral plane. Right image: Laser light image of FZP focus.

4.3 Testing for variation of FZP focal point intensity with device motion

The 4-ring spiral FZP shown in Figure 12 was tested. An IR black-body source was placed as shown in Figure 10 such that an image of the source was formed at the FZP. The temperature of the IR source was set to 500 C, and no chopper was used. The pinhole and microscope were adjusted to give an image of the FZP focus spot on the CCD. The IR source was first blocked and the CCD captured images at a rate of 48.4 frames per second for 5 seconds. The test was repeated with the IR source unblocked. The data was analyzed by examining a 4x4 pixel region enclosing the FZP focus spot in each image. The average pixel value is displayed as a function of time in Figure 13 for both the blocked and unblocked IR tests. A consistent and repeatable difference between the blocked and unblocked data was seen.

As a second test, the IR black-body source was replaced by a soldering iron with the tip temperature set at 550 C. A chopper was placed as shown in Figure 10 and the frequency of the chopper was set at 4.1 Hz. The CCD again captured images at a sample rate of 48.4 Hz. A three second sample of the average pixel intensity value for a 3x3 pixel area containing the FZP focus spot is plotted in Figure 14. A Fourier transform of this data is shown in Figure 15 where the peak at the 4.1 Hz chopping frequency is clearly visible.

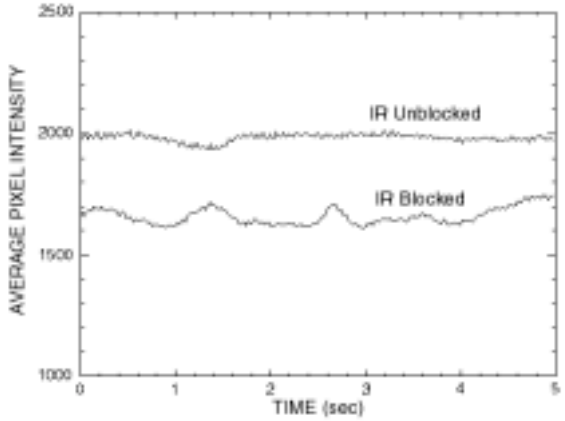

Figure 13. Average intensity of the FZP focus spot when the IR is blocked and unblocked.

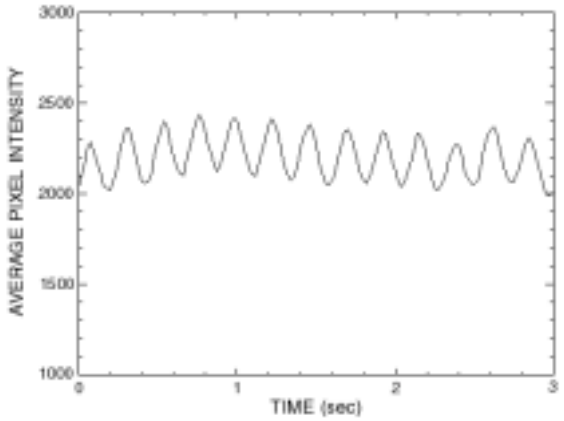

Figure 14. FZP focus spot brightness as the bi-material cantilever responds to the IR radiation from a soldering iron. The radiation is chopped at 4.1 Hz.

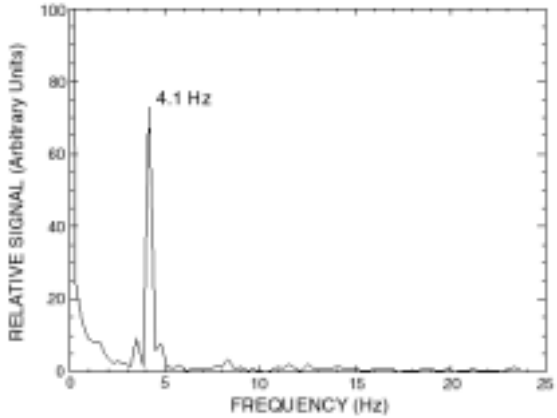

Figure 15. Fourier transform of the data in Figure 14. Note the peak at the chopping frequency.

4.4 Active pixel with integrated FZP for IR imaging

In Figure 14 a slight drift in the intensity can be seen over the span of several seconds. On longer scans of several minutes, these fluctuations can be on the order of or larger than the signal. In the Fourier transform however, the amplitude of the peak at the chopping frequency corresponds very well with the amplitude of the short period peak-to-peak changes seen in Figure 14. The long period noise shows up at lower frequency and can be ignored. To make an image of a hot object with this device will take many minutes. We therefore make use of this Fourier technique to extract consistent data over these long scan periods.

On the left of Figure 16 is an IR image of a soldering iron tip at 450 C. Below the IR image is a photo of the tip shown to the same scale for comparison. The IR image resolution is 20x20 pixels. The soldering iron tip was rastered in a 20x20 x-y grid. At each point the tip was stopped and the CCD captured 256 images of the FZP focus spot at a rate of 48.4 Hz. The chopper was operated at 4.3 Hz. From the 256 images, the average pixel intensity was extracted as in Figure 14, the Fourier transform was

taken as in Figure 15, and the 4.3 Hz component of the transform was recorded as the pixel value in the IR image at that x,y position. On the right of Figure 16 is a similar IR image of a thin metal structure added to the soldering iron tip at 450 C. Below the IR image is a photo of the object shown to the same scale for comparison.

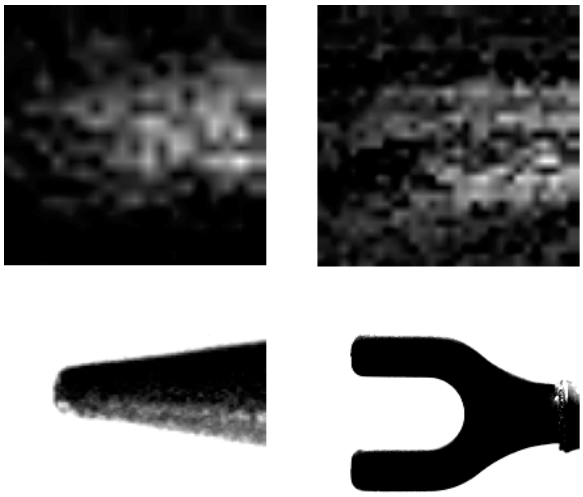

Figure 16. IR images produced with a pixel with integrated spiral FZP. Top images are the IR images of the objects shown directly below to the same scale. Left side is a soldering iron tip. Right side is a metal shape attached to the same soldering iron tip (not shown).

5. DISCUSSION

The fabrication of the basic substrate structures used here (square pixel and triangular cantilever) was found to be accurate and reproducible, however, the diffractive micro-optical elements proved to be more difficult to produce accurately and consistently. These structures must be very precise to produce the desired diffractive effects. Rough edges on the diffractive features produce diffractive noise and very small variations from the theoretical radii of the rings of the FZP lead to changes in the intensity profile and focus distance of the device. The pixel with 4-ring spiral FZP (Section 3.3) has a focus distance within 10% of the theoretical calculation, but the triangular cantilever with 4-ring spiral FZP (Section 3.5) was found to have a focal distance of almost twice the expected value. Comparing Figure 8 with Figure 6 it appears that the spacing of the milled out region is a little wider in the triangular cantilever version, possibly leading to the increased focal length.

Fortunately, for our purposes the location of the FZP focus is not as important as is the intensity profile of the focus and that appears very promising. For the intensity data shown in Figure 13 the difference in average pixel intensity between the IR blocked and the IR unblocked is about 300. Since this average is over 16 pixels this corresponds to 4800 intensity levels between the room temperature (IR blocked) and the 550 C temperature of the soldering iron (IR unblocked) for a sufficiently high signal to noise ratio. This device is also mounted in open air which carries away heat and causes mechanical turbulence. Mounting the device in vacuum should provide much higher temperature sensitivity and lower noise. Our first attempts to use the devices to create the IR images in Figure 16 are also encouraging as the basic shapes of the hot objects are clearly visible even though the pixel resolution is small (20x20). With increased resolution and placing the device in vacuum the images will certainly improve.

Also, though we have had great success in fabricating the circular FZP in the coatings on the SiNx substrate, the focal spot is very poorly defined. The surface of the SiNx may be roughened by the milling process causing diffractive noise. The precision fabrication required by the circular FZP may best be achieved by conventional semiconductor processing techniques. Figure 17 shows a small portion of a mask used for the first step in such a process. The mask is for a 64x64 array of 8-ring circular FZP

pixels. The mask is a thin chromium and gold layer on a quartz substrate and was produced using electron-beam lithography. The FZPs in the mask have a primary radius R_1 = 40 μm. When illuminated by a HeNe laser, the calculated focus distance is 2.528 mm. The focus distance obtained experimentally with this mask was 2.53 mm. In the next step of the conventional semiconductor process this mask will be reduced by a factor of ten to produce actual devices with R_1 = 4 μm and a focus distance of 25.3 μm.

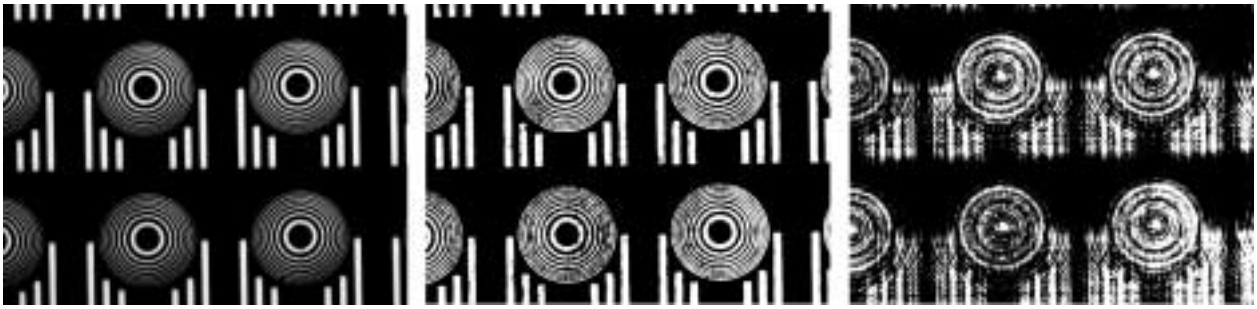

Figure 17. Portion of a mask for producing a 64x64 array of 8-ring circular FZP pixels. LEFT: White light CCD image. CENTER: Same section illuminated by laser light, CCD focused at device plane. RIGHT: Same as center but focused at the primary focus distance and showing the FZP focus spot at center of each pixel.

We have successfully fabricated micro FZP diffractive features on MEMS structures. The spiral FZP diffractive features produce well defined foci whose intensity varies with distance from the FZP. Observation of these intensity variations have enabled us to detect the motion of the MEMS structure, and the resulting device has been used to scan an IR image of a hot object. Though our current motion detection success has been limited to the spiral FZP feature, the added precision of the photolithographic process described above (Figure 17) will result in circular FZP with sharply defined foci which will allow more sensitive discrimination of device motion.

ACKNOWLEDGMENTS

The work performed by Oak Ridge National Laboratory was supported by DARPA, and the Laboratory Director's Research and Development Program of Oak Ridge National Laboratory. Oak Ridge National Laboratory is operated for the U.S. Department of Energy by UT-Battelle, LLC, under contract DE-AC05-00OR22725. The work performed by the University of Tennessee was supported by the NSF grant ECS-9727208.

REFERENCES

[1] D. Sarid, *Scanning Force Microscopy* (Oxford University Press, New York, 1991).
[2] E. Hecht, *Optics* 2nd Edition, pp. 445-446 (Addison Wesley, Reading Massachusetts, 1987).
[3] P. G. Datskos, S. Rajic, L. R. Senesac, D. D. Earl, B. M. Evans, J. L. Corbeil, and I, Datskou, "Optical readout of uncooled thermal detectors," Infrared Technology and Applications XXVI, SPIE **4130**, 185 (2000).
[4] P. G. Datskos, S. Rajic, and I. Datskou, "Photoinduced and thermal stress in silicon microcantilevers," Applied Physics Letters **73**, 16 (1998).